Formulation of Chromatin Mobility as a Function of Nuclear Size during *C. elegans* Embryogenesis Using Polymer Physics Theories

Aiya K. Yesbolatova[1,2] Ritsuko Arai[2,*] Takahiro Sakaue[3,†] and Akatsuki Kimura[1,2,‡]

[1]*Department of Genetics, School of Life Science, The Graduate University for Advanced Studies, SOKENDAI, Mishima 411-8540, Japan*

[2]*Cell Architecture Laboratory, Department of Chromosome Science, National Institute of Genetics, Mishima 411-8540, Japan*

[3]*Department of Physical Sciences, Aoyama Gakuin University, 5-10-1 Fuchinobe, Chuo-ku, Sagamihara, Kanagawa 252-5258, Japan*

During early embryogenesis of the nematode, *Caenorhabditis elegans*, the chromatin motion markedly decreases. Despite its biological implications, the underlying mechanism for this transition was unclear. By combining theory and experiment, we analyze the mean-square displacement (MSD) of the chromatin loci, and demonstrate that MSD-vs-time relationships in various nuclei collapse into a single master curve by normalizing them with the mesh size and the corresponding time scale. This enables us to identify the onset of the entangled dynamics with the size of tube diameter of chromatin polymer in the *C. elegans* embryo. Our dynamical scaling analysis predicts the transition between unentangled and entangled dynamics of chromatin polymers, the quantitative formula for MSD as a function of nuclear size and timescale, and provides testable hypotheses on chromatin mobility in other cell types and species.

How does chromatin move? This question has attracted broad interest in both the fundamental and applied sciences, from biology to physics. While chromatin moves, in some case, in a directional manner [1], its motion is mostly stochastic. Such stochastic motions are associated with the biological functions. For instance, chromatin motion in the timescale of $\tau \simeq 0.1$–1 s is known to correlate with the activity of transcription [2]. Larger scale motion, $\tau \simeq 10$–100 s, increases upon DNA damage, and this increase is considered to facilitate a homology search for recombination repair [3]. In addition, such large scale motion is known to slow down as the cell division proceeds during the embryogenesis of *C. elegans* [4]. The reduction in mobility correlated with the formation of heterochromatin and nucleoli [4,5], suggesting the contribution of chromatin mobility to the global nuclear organization. The mechanism causing the reduction of mobility during embryogenesis is yet elusive.

Polymer physics has been successful to describe several fundamental aspects of chromatin [6–10]. The theory, however, behind the relationship between the chromatin mobility and the nuclear size is yet to be established. In characterizing chromatin motion, one usually calculates from the erratic trajectory $\vec{r}(t)$ the mean-square displacement (MSD): $\langle (\vec{r}(t_0 + \tau) - \vec{r}(t_0))^2 \rangle$, where the averaging is taken over the time of origin t_0 and/or the different nuclei [11]. Previous experiments have reported that, in many cases, the MSD of chromatin loci exhibits a power-law dependence on the lag-time τ;

$$\mathrm{MSD}(\tau) = A\tau^\alpha. \tag{1}$$

The MSD exponent α typically falls in the range $\alpha < 1$ [6,12–14], indicating that the diffusion of chromatin loci is anomalous due primary to the polymeric nature of chromatin [7,15–18]. According to the theory of polymer dynamics, the simplest model (Rouse model), which takes the connectivity of segments into account, predicts $\alpha = 0.5$. Inclusion of the hydrodynamic interactions between distant segments (Zimm model) enhances the exponent to $\alpha = 2/3$, while the motional restriction due to the entanglement effect results in the slowing down in dynamics $\alpha < 0.5$ [19–21].

Given the complexity in the cellular nucleus, however, one naturally asks the relevance of such simple models, or more crucially, the circumstances under which each model applies. The early embryo, where the chromatin organization is relatively simple, provides an ideal system to apply a polymer physics approach without unnecessary complications. Indeed, in the early embryo of *C. elegans*, chromatin is distributed almost uniformly in the nucleus, as judged from histone distribution [4]. No clear sign of topologically associating domains (TADs) was observed in autosomes [22]. In the present study, we identify the mesh size, a fundamental length scale in polymer solution as a function of the nuclear size, and demonstrate that the apparently different MSD data from nuclei of various sizes can be collapsed onto a single master curve. This leads us to conclude that the essential aspect of the chromatin dynamics in *C. elegans* embryo can be well described by a simple polymer physics model. Our finding emphasizes the importance of the spatiotemporal viewpoint in chromatin dynamics, where the nuclear size affects the characteristic

length and timescales. In addition, we speculate the deviation from the current simple model may probe the establishment of higher order structures in differentiated nuclei.

Relationship between chromatin mobility and nuclear size.—Following the previous study, we visualized the *lacO* locus integrated into a pair of sister chromosomes in the *C. elegans* genome using the LacI-GFP fusion protein [4,23] (Fig. S1, Supplemental Material, movie S1 [24]). The distribution of the *lacO* spots follows random distribution [4], in contrast to the peripheral localization of the telomeres [40]. The tracking analysis of a single locus may lead to an erroneous interpretation, because of a possible influence caused by the motion of the nucleus. This is indeed the case in our experiment, where the apparent motion of a locus is dominated by the nucleus motion (Fig. S2, Supplemental Material [24]). To exclude such an extrinsic effect, we track the positions $\vec{r}_1(t)$ and $\vec{r}_2(t)$ of the pair of *lacO* spots in sister chromosomes, and calculate the distance $d(t) = \sqrt{(\vec{r}_2(t) - \vec{r}_1(t))^2}$ between them. From the time series of $d(t)$, we deduce the mean square change in distance (MSCD) as a function of lag-time τ [3,4];

$$\text{MSCD}(\tau) = \langle (d(t_0 + \tau) - d(t_0))^2 \rangle. \quad (2)$$

Intuitively, one may suppose that MSCD behaves similarly to the MSD. Indeed, several past studies employed MSCD to quantify the chromatin dynamics [4,41], but its precise relation to MSD has not been addressed. We devise a formula relating these two quantities $\text{MSD} = d_0^2 [\{f(\text{MSCD}/d_0^2)\}^{-4} + \{g(\text{MSCD}/d_0^2)\}^{-4}]^{-\frac{1}{4}}$, where $f(Y) = \frac{3}{2}Y$ and $g(Y) = (Y/2) + \sqrt{Y}$ and $d_0 = d(t_0)$ (Fig. S3; see Supplemental Material [24] for a derivation), and convert the measured MSCD to MSD.

To focus on the relationship between the nuclear size (radius R) and chromatin mobility (MSD), we first group nuclei of similar sizes (i.e., $0.4 \times i - 0.2 \leq R \, [\mu m] < 0.4 \times i + 0.2$, $i = 1, 2, 3....$), and fit the MSD data from each group of nuclei to Eq. (1) [Fig. 1(a), solid lines]. The MSD exponent α has a weak correlation with R [Fig. 1(b) (blue), the coefficient of determination $r^2 = 0.55$, $p = 0.06$]. The MSD exponents are near 0.5 [Fig. 1(b), blue dotted line], which is expected from the Rouse model. In smaller nuclei, however, we notice $\alpha < 0.5$. Later in this study, we will elaborate the size dependency of the exponent. For the moment, we tentatively compare the chromatin mobility by fitting the MSD data for each group of nuclei to Eq. (1) by fixing the exponent to the Rouse model value $\alpha = 0.5$ [Fig. 1(a), dotted lines]. The amplitude, or the so-called generalized diffusion coefficient obtained ($A_{0.5}$) exhibits a clear trend against nuclear size, in that it takes a smaller value for smaller R [Fig. 1(b) (red), $r^2 = 0.96$, $p = 9 \times 10^{-5}$]. These results demonstrate a correlation between chromatin mobility and nuclear size. As embryonic development is accompanied by a reduction
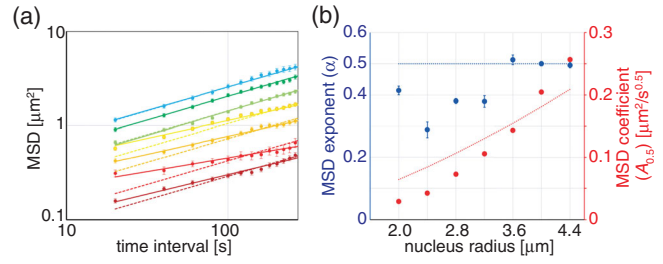

FIG. 1. Chromatin mobility correlates with nuclear size. (a) MSD of different nuclei sizes. Different colors represent different sizes of nuclei. Nuclear radius = 2.0 (brown), 2.4 (red), 2.8 (orange), 3.2 (yellow), 3.6 (light green), 4.0 (green), 4.4 (light blue), [μm]. The solid lines represent fitting to Eq. (1), whereas the dotted lines are fitting to Eq. (1) with α fixed to 0.5. (b) MSD exponent α (blue) and MSD coefficient A (assuming the constant exponent of $\alpha = 0.5$, red) of each group. The error bars represent S.D (standard deviation). The blue dotted line indicates $\alpha = 0.5$, and the red dotted curve represents a fit $A_{0.5} \sim R^{1.5}$, which are expected from the Rouse dynamics.

in nuclear size, the present result is consistent with the previously established correlation between chromatin mobility and the early embryonic stage [4].

To verify whether changes in nuclear size can cause changes in chromatin motion in a cell-stage independent manner, we induce changes in nuclear size using genetic manipulation. RNA-mediated interference (RNAi) of *ima-3* and *C27D9.1* genes induce smaller and larger nuclear sizes, respectively [5,42]. We focus on the eight-cell stage, which may correspond to a transition from high to low mobility of the chromatin [4]. The RNAi of the *ima-3* and *C27D9.1* genes widens the range of nuclear size [Fig. 2(a)]. We plot the amplitude of the chromatin motion $A_{0.5}$ only from the eight-cell stage nuclei [Fig. 2(b), filled circles]. We detected a clear correlation between the chromatin motion and the nuclear size even in a same cell stage [Fig. 2(b), $r^2 = 0.94$, $p = 0.001$], with a trend similar to the control cells from
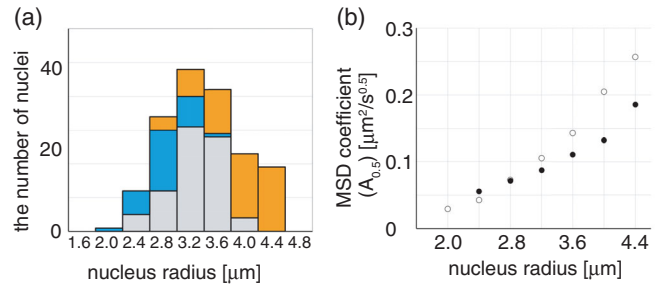

FIG. 2. Changes in nuclear size induce changes in chromatin motion. (a) Distribution of the radii of nuclei in the eight-cell stage. Control (gray), *ima-3* (RNAi) (blue), and *C27D9.1* (RNAi) (orange). (b) Correlation between the MSD coefficient and the nuclear radius in the eight-cell stage (filled circle). Blank circles represent the MSD coefficient calculated from all stages as shown in Fig. 1(b). The error bars represent S.D.

various stages [Fig. 2(b), blank circles]. The result supports our hypothesis that chromatin mobility depends on nuclear size.

Modeling intranuclear chromatin as polymer solution.— We now discuss the physics underlying the nuclear size dependence of chromatin mobility. Our estimate [24] indicates that the chromatin at these stages is best described as a semidilute polymer solution, a state where the polymer chains are strongly overlapping but not concentrated too much [19–21]. The mobility of the chromatin locus will be affected by the concentration c of chromatin segment, when the locus moves large enough to encounter surrounding chromatin polymers. This statement can be explicitly formulated based on the notion of the mesh size ξ, which is the characteristic length scale in semidilute polymer solution [Fig. 3(a)]. Using the mesh size ξ, one can write the MSD of the chromatin locus as

$$\mathrm{MSD}(\tau) = \xi^2 \left(\frac{\tau}{\tau_\xi}\right)^\alpha, \tag{3}$$

where τ_ξ is the timescale corresponding to the mesh size, and regime-dependent exponent α characterizes the dynamics in the corresponding regime; as we discuss below α takes distinct values for τ smaller or larger than τ_ξ.

How do the mesh size ξ depends on the nuclear size? Let g be a number of segments inside each mesh. The chromatin conformation within mesh will be described by $\xi \simeq l g^{1/2}$, where l is the Kuhn length of chromatin. Since the meshes are space filling $g/\xi^3 \simeq c$, one finds $\xi \simeq l^{-2} c^{-1}$. Here, we assume the random walk chromatin conformation as the chromatin segment is rather slender, i.e., its Kuhn length l ($\simeq 100$ nm) is larger than its radius b ($\simeq 10$ nm), making the excluded volume effect irrelevant [43,44] (see Fig. S4 in the Supplemental Material [24] for the effect of self-avoidance). With the concentration $c \simeq (3/4\pi)MR^{-3}$ of the segments, where M is the total number of segments inside the nucleus, we find

$$\xi \simeq (4\pi/3) l^{-2} M^{-1} R^3. \tag{4}$$

The estimated mesh size as a function of nuclear size is summarized in Fig. 3(b), where we adopt $M = 100\,000$ based on the amount of DNA per nucleus to be $\simeq 400$ Mbp and the estimated segment size of $\simeq 4$ kb [24]. The corresponding timescale τ_ξ is found by noting the relevance of hydrodynamics interactions inside the mesh, where the so-called Zimm dynamics applies $\tau_\xi \simeq \eta \xi^3 / k_B T$ [19–21]. Here $k_B T$ and η are the thermal energy and viscosity of the solvent (nucleoplasm), respectively (see Fig. S4 in Ref. [24] for the effect of hydrodynamic interaction). This gives the nuclear size dependency of τ_ξ as

$$\tau_\xi \simeq \{64\pi^3 \eta / (27 k_B T)\} l^{-6} M^{-3} R^9. \tag{5}$$

(a)

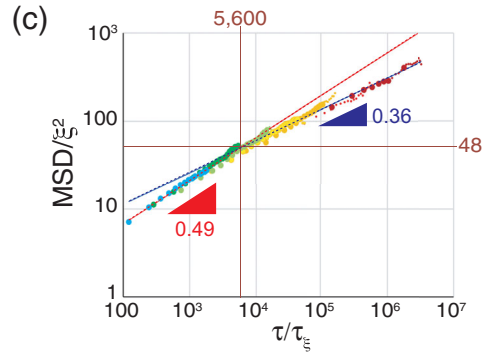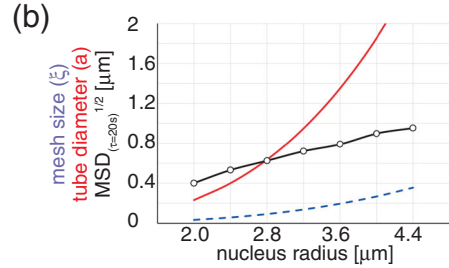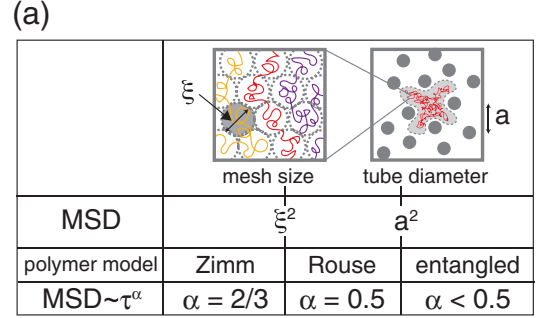|	mesh size	tube diameter	
MSD	ξ^2	a^2	
polymer model	Zimm	Rouse	entangled
MSD~τ^α	$\alpha = 2/3$	$\alpha = 0.5$	$\alpha < 0.5$

(b)

(c)

FIG. 3. (a) Summary of the relationship among MSD, mesh size ξ, tube diameter a, time- and nuclear-size dependencies of MSD discussed in the text. Top schematics illustrate the mesh size and the tube diameter in the chromatin solution. (b) Quantitative comparison of the mesh size, tube diameter and MSD in different nuclear size. The mesh size ξ (blue dotted line) is calculated according to Eq. (4) as $\xi = 4.2 \times 10^{-3} \times R^3$ [μm]. The tube diameter estimated from the experiment (red solid line) as the border of the broken line in Fig. S5 [24] is $a = \xi \times 48^{1/2} = 2.9 \times 10^{-2} \times R^3$ [μm]. Black line is MSD$^{1/2}$ at $\tau = 20$ s obtained from the experiment [Fig. 1(a)]. (c) The master curve of MSD constructed by time-nuclear size superposition (double logarithmic scale) by normalizing MSD and τ by ξ^2 and τ_ξ, respectively. The color code is the same as in Fig. 1(a). The broken line on the plot is obtained by fitting the plot as described in Ref. [24]. The larger spots correspond to the measurements with S.E.M./MSD ≤ 0.06, whereas the others are shown with the smaller spots.

Substituting Eqs. (4) and (5) into Eq. (3), we obtain nuclear size dependence in MSD $\sim A\tau^\alpha$ of chromatin loci,

$$A \sim R^{6-9\alpha}. \tag{6}$$

Importantly, the exponent for the nuclear size dependence is a function of the temporal exponent α. Since the

latter depends on the length scales and timescales (see below), the nuclear size dependence of MSD also reflects the spatiotemporal structure of the chromatin polymer solution. For the length scale smaller than the mesh size ξ, the Zimm dynamics predicts the MSD temporal exponent $\alpha = 2/3$ [19–21] [Fig. 3(a)]. In this case, $\mathrm{MSD} \sim R^0$ [Eq. (6)], which is not the case in our experiment. For the length scale larger than ξ, the hydrodynamic interactions are screened, and the so-called Rouse dynamics applies, hence, $\alpha = 0.5$ [19–21]. In this case $\mathrm{MSD} \sim R^{1.5}$ according to Eq. (6). Thus, the Rouse dynamics scenario provides the temporal exponent roughly consistent with the α in our experiment [Fig. 1(b), blue], and the experimentally found positive correlation between the MSD coefficient $A_{0.5}$ and the nuclear size R [Fig. 1(b), red]. However, we notice $\alpha < 0.5$ for smaller nuclei [Fig. 1(b), blue], and the actual nuclear size dependence is stronger than the Rouse model prediction [$A_{0.5} \sim R^{1.5}$, Fig. 1(b), red dotted line], which indicates the presence of another physical mechanism at work.

Master curve and crossover to entangled dynamics.— We replotted Fig. 1(a) by normalizing MSD and τ with ξ^2 and τ_ξ, respectively, to obtain the dimensionless plot [Fig. 3(c)]. The rescaled plot indicates that the MSD obtained in this study is larger than the estimated mesh size squared (ξ^2) [Figs. 3(b) and 3(c)]. This means that chromatin motion measured in this study is theoretically large enough to be dependent on chromatin concentration c, and thus on nuclear size R. More importantly, the MSD data from nuclei with various sizes converges to a single *master curve*, which captures the relationship between the chromatin mobility and the nuclear size in a broad range of time and spatial scales.

As already mentioned, the experimentally found R dependence of MSD is stronger than the Rouse model prediction [Fig. 1(b)]. In addition, a close inspection of the master curve [Fig. 3(c)] reveals the finer structure of the temporal exponent. While the shorter timescale part has a slope $\alpha = 0.486 \pm 0.007$ (S.D.) consistent with the Rouse model, the longer timescale dynamics is characterized by a smaller exponent $\alpha = 0.359 \pm 0.003$ (S.D.). $\alpha < 0.5$, and thus $6 - 9\alpha > 1.5$ in Eq. (6), is consistent with stronger nuclear size dependency on MSD [compare red spots with red dotted line in Fig. 1(b)]. It is also consistent with smaller slopes of the MSD-vs-τ curve than those expected for $\alpha = 0.5$ [dotted lines in Fig. 1(a), yellow or lower] and $\alpha < 0.5$ in Fig. 1(b) (blue spots) for smaller nuclei with $R \leq 3.2~\mu\mathrm{m}$.

From a broken-line fitting of Fig. 3(c), we identify the crossover point at $(\tau/\tau_\xi, \mathrm{MSD}/\xi^2) = (5600 \pm 600, 48 \pm 2)$ (best fit values $\pm$ S.D.). We propose that the spatial scale of this crossover corresponds to the tube diameter of chromatin solution in living *C. elegans* embryos [Fig. 3(a)]. The tube diameter is the length scale, at which the topological (noncrossability) constraint starts to affect the polymer

behaviors [19–21]. Our data lead to the nuclear size-dependent tube diameter $a = k_1 \times R^3$ [$\mu\mathrm{m}$] [Fig. 3(b)] and the corresponding time scale $\tau_a = k_2 \times R^9$ [s], where $k_1^2 = (8.4 \pm 0.4) \times 10^{-4}$ [$\mu\mathrm{m}^{-4}$] and $k_2 = (1.5 \pm 0.2) \times 10^{-3}$ [s/$\mu\mathrm{m}^{-9}$] (best fit value $\pm$ S.D.) with R measured in $\mu\mathrm{m}$. Thus, the experimentally determined tube diameter a is found to be $\sim 48^{1/2}$ times larger than the theoretically estimated mesh size ξ. This ratio is consistent with the often invoked estimate (~ 10) [24]. Combined with the generic formula Eq. (3), this gives us

$$\mathrm{MSD}(\tau, R) = \left(\frac{k_1^2}{k_2^\alpha}\right) \tau^\alpha R^{6-9\alpha}, \qquad (7)$$

where $\alpha = 0.49$ for $0.02 \leq \tau/\tau_a \leq 1$, $\alpha = 0.36$ for $1 \leq \tau/\tau_a \leq 600$ (Fig. S5 in the Supplemental Material [24]). This represents the quantitative relationship among the chromatin mobility (MSD), timescale (τ), and the nuclear size (R) in the *C. elegans* embryo.

Discussion.—Nuclear size has been reported to affect the formation of nucleoli [5] and chromosome condensation [42]. Here we show that nuclear size also affects the mobility of chromatin in the early *C. elegans* embryo on the timescale of ≥ 20 s. We have found that the chromatin loci explores the spatial scale larger than the estimated mesh size in the nuclei, and thus the mobility should depend on the chromatin concentration, hence, nuclear size. In addition, the MSD in smaller nucleus and/or in the longer timescales exceeds the tube diameter of the chromatin solution, where the entanglement slows down the dynamics, and make the mobility more sensitive to nuclear size.

A mechanism for the entangled dynamics leading to the exponent $\alpha = 0.36$ is currently unclear. As a classical example, the reptation theory predicts the substantial slowing down $\alpha = 0.25$ in the entangled linear polymer solution [19–21], but this theoretical value could often be blurred by the crossover effect, resulting in a slightly larger value. In addition, different mechanisms, for instance, relevant to nonconcatenated ring polymers [9,45–52], result in different exponents.

The transition from unentangled to entangled dynamics was observed around the nucleus with $R \simeq 3~\mu\mathrm{m}$ [Figs. 1(b) and 3(b)]. This size corresponds to the eight-cell stage of the embryogenesis [Fig. 2(a)]. We propose that the entanglement effect is dominant in chromatin movement on the time scale ≥ 20 s in eight-cell stage or later. Interestingly, the eight-cell stage of the *C. elegans* embryo is when the nucleoli and other chromatin structures start to appear [4,5], and when the major transcription from zygotic genome starts [53]. We speculate that the start of entangled dynamics of chromatin polymer induced by the physical constraint of nuclear size triggers the massive reorganization of the nucleus leading to the change in nuclear activities.

The apparent success of simple modeling based on polymer physics concept likely reflects a primitive, uniform chromatin structure in the early *C. elegans* embryo. It is interesting to examine the chromatin dynamics in embryos of different species. Similar models may apply to chromatin in undifferentiated cells such as stem cells. Moreover, the applicability of our model may provide a useful index reflecting the differentiation status of chromatin.

Finally, from methodological viewpoint, we propose a general workflow to analyze chromatin mobility in living cells. We evaluated the contribution of the nuclear movement by two-point correlation tracking (Fig. S2 in Ref. [24]). We developed a method to estimate the intrinsic MSD of chromatin excluding the effect of the nuclear movement (Fig. S3 in Ref. [24]). By normalizing MSD and time with an estimated mesh size ξ and the corresponding timescale τ_ξ, we found the transition from the unentangled to the entangled dynamics [Fig. 3(c)]. Fitting of the scaling plot allowed us to formulate the mobility and estimate the relevant parameters [Eq. (7)]. We expect that our analyses workflow has versatile applicability to the quantification of intrinsic chromatin mobility in living cells.

---

[*]Present address: Department of Anatomy and Histology, Fukushima Medical University, School of Medicine, 1 Hikarigaoka, Fukushima 960-1295, Japan.

[†]sakaue@phys.aoyama.ac.jp

[‡]akkimura@nig.ac.jp

[1] Y. Hiraoka and A. F. Dernburg, Dev. Cell **17**, 598 (2009).

[2] R. Nagashima, K. Hibino, S. S. Ashwin, M. Babokhov, S. Fujishiro, R. Imai, T. Nozaki, S. Tamura, T. Tani, H. Kimura *et al.*, J. Cell Biol. **218**, 1511 (2019).

[3] J. Miné-Hattab and R. Rothstein, Nat. Cell Biol. **14**, 510 (2012).

[4] R. Arai, T. Sugawara, Y. Sato, Y. Minakuchi, A. Toyoda, K. Nabeshima, H. Kimura, and A. Kimura, Sci. Rep. **7**, 3631 (2017).

[5] S. C. Weber and C. P. Brangwynne, Curr. Biol. **25**, 641 (2015).

[6] H. Hajjoul, J. Mathon, H. Ranchon, I. Goiffon, J. Mozziconacci, B. Albert, P. Carrivain, J. M. Victor, O. Gadal, K. Bystricky, and A. Bancaud, Genome Res. **23**, 1829 (2013).

[7] T. Sakaue and T. Saito, Soft Matter **13**, 81 (2017).

[8] J. D. Halverson, J. Smrek, K. Kremer, and A. Y. Grosberg, Rep. Prog. Phys. Phys. Soc. (Great Britain) **77**, 022601 (2014).

[9] A. Rosa and R. Everaers, PLoS Comput. Biol. **4**, e1000153 (2008).

[10] S. Brahmachari and J. F. Marko, Proc. Natl. Acad. Sci. U.S.A. **116**, 24956 (2019).

[11] E. Barkai, Y. Garini, and R. Metzler, Phys. Today **65**, 29 (2012).

[12] I. Bronstein, Y. Israel, E. Kepten, S. Mai, Y. Shav-Tal, E. Barkai, and Y. Garini, Phys. Rev. Lett. **103**, 018102 (2009).

[13] S. C. Weber, A. J. Spakowitz, and J. A. Theriot, Phys. Rev. Lett. **104**, 238102 (2010).

[14] S. C. Weber, A. J. Spakowitz, and J. A. Theriot, Proc. Natl. Acad. Sci. U.S.A. **109**, 7338 (2012).

[15] A. Amitai and D. Holcman, Phys. Rev. E **88**, 052604 (2013).

[16] H. Vandebroek and C. Vanderzande, Phys. Rev. E **92**, 060601(R) (2015).

[17] K. E. Polovnikov, M. Gherardi, M. Cosentino-Lagomarsino, and M. V. Tamm, Phys. Rev. Lett. **120**, 088101 (2018).

[18] S. Put, T. Sakaue, and C. Vanderzande, Phys. Rev. E **99**, 032421 (2019).

[19] P. G. de Gennes, *Scaling Concepts in Polymer Physics* (Cornell University Press, Ithaca, 1979).

[20] M. Doi and S. F. Edwards, *The Theory of Polymer Dynamics*, International Series of Monographs on Physics (Oxford University Press, Oxford, 1986).

[21] M. Rubinstein and R. Colby, *Polymer Physics* (Oxford University Press, Oxford, 2003).

[22] E. Crane, Q. Bian, R. P. McCord, B. R. Lajoie, B. S. Wheeler, E. J. Ralston, S. Uzawa, J. Dekker, and B. J. Meyer, Nature (London) **523**, 240 (2015).

[23] C. Bilgir, C. R. Dombecki, P. F. Chen, A. M. Villeneuve, and K. Nabeshima, G3 (Bethesda) **3**, 585 (2013).

[24] See Supplemental Material at http://link.aps.org/supplemental/10.1103/PhysRevLett.128.178101 for methods, figures, table, movie, and additional theoretical discussions, which includes Refs. [25–39].

[25] S. Brenner, Genetics **77**, 71 (1974).

[26] A. Zidovska, D. A. Weitz, and T. J. Mitchison, Proc. Natl. Acad. Sci. U.S.A. **110**, 15555 (2013).

[27] A. Kimura, A. Celani, H. Nagao, T. Stasevich, and K. Nakamura, Front. Phys. **6**, 60 (2015).

[28] H. Kang, Y.-G. Yoon, D. Thirumalai, and C. Hyeon, Phys. Rev. Lett. **115**, 198102 (2015).

[29] J. Dekker, K. Rippe, M. Dekker, and N. Kleckner, Science **295**, 1306 (2002).

[30] J. Langowski, Eur. Phys. J. E **19**, 241 (2006).

[31] M. Tark-Dame, R. v. Driel, and D. W. Heermann, J. Cell Sci. **124**, 839 (2011).

[32] M. Bohn and D. W. Heermann, PLoS One **5**, e12218 (2010).

[33] K. Bystricky, P. Heun, L. Gehlen, J. Langowski, and S. M. Gasser, Proc. Natl. Acad. Sci. U.S.A. **101**, 16495 (2004).

[34] J. Dekker and B. v. Steensel, *Handbook of Systems Biology* (Academic Press, San Diego, 2012), pp. 137—151.

[35] L. G. Edgar and J. D. McGhee, Cell **53,** 589 (1988).

[36] L. Liang, X. Wang, D. Xing, T. Chen, and W. R. Chen, J. Biomed. Opt. **14,** 024013 (2009).

[37] N. Uchida, G. S. Grest, and R. Everaers, J. Chem. Phys. **128,** 044902 (2008).

[38] Y. H. Lin, Macromolecules **20,** 3080 (1987).

[39] T. A. Kavassalis and J. Noolandi, Phys. Rev. Lett. **59,** 2674 (1987).

[40] H. C. Ferreira, B. D. Towbin, T. Jegou, and S. M. Gasser, J. Cell Biol. **203,** 727 (2013).

[41] J. S. Lucas, Y. Zang, O. K. Dudko, and C. Murre, Cell **158,** 339 (2014).

[42] Y. Hara, M. Iwabuchi, K. Ohsumi, and A. Kimura, Mol. Biol. Cell **24,** 2442 (2013).

[43] D. W. Schaefer, J. F. Joanny, and P. Pincus, Macromolecules **13,** 1280 (1980).

[44] T. Sakaue, Macromolecules **40,** 5206 (2007).

[45] M. E. Cates and J. M. Deutsch, J. Phys. (Paris) **47,** 2121 (1986).

[46] T. Sakaue, Phys. Rev. Lett. **106,** 167802 (2011).

[47] J. Smrek and A. Y. Grosberg, J. Phys. Condens. Matter **27,** 064117 (2015).

[48] T. Ge, S. Panyukov, and M. Rubinstein, Macromolecules **49,** 708 (2016).

[49] D. Michieletto, N. Nahali, and A. Rosa, Phys. Rev. Lett. **119,** 197801 (2017).

[50] T. Sakaue, Soft Matter **14,** 7507 (2018).

[51] F. Landuzzi, T. Nakamura, D. Michieletto, and T. Sakaue, Phys. Rev. Research **2,** 033529 (2020).

[52] D. Michieletto and T. Sakaue, ACS Macro Lett. **10,** 129 (2021).

[53] L. G. Edgar, N. Wolf, and W. B. Wood, Development **120,** 443 (1994).